State-Plane Analysis of Regenerative Snubber for Flyback Converters

Article *in* IEEE Transactions on Power Electronics · November 2013

DOI: 10.1109/TPEL.2013.2243845

3 authors, including:

Alexander Abramovitz
University of California, Irvine
100 PUBLICATIONS **1,677** CITATIONS

State Plane Analysis of Regenerative Snubber for Flyback Converters

***Abstract*— the flyback converter is a popular topology for implementing low power multiple output power supplies. However, the high leakage inductance of the flyback transformer causes high voltage spikes that can damage the main transistor when the switch is turned off. Therefore, a turn-off snubber is needed to limit the peak voltage stress. This paper presents the analysis of an energy regenerative snubber using the graphical state plane technique. The undertaken approach yields a clear-cut design procedure for minimum switch voltage stress. Experimental evaluation of the energy regenerative snubber in comparison with other common snubbers shows that under the same voltage stress the efficiency of energy regenerative snubber has 8% improvement in average over RCD snubber and 2% improvement over non-dissipative LC snubber.**

***Index Terms*— snubber, regeneration, protection, flyback converter**

I. Introduction

A notable advantage of the flyback converter is its low component count. Flyback is a single switch topology that makes use of only one magnetic component to attain both the isolation and energy transfer [1], [2]. Moreover, the low-cost and rugged flyback converter can provide both step-up and step-down conversion and, for these reasons, it is the designer's choice in low-power multiple output applications.

One challenge in designing of the flyback converter is handling the energy, trapped in the leakage inductance of the flyback transformer. As the main transistor is turned off, the discharge of leakage energy develops high voltage spike across the switch and can cause destruction. The conventional RCD snubber, shown in Fig. 1 (a), is a simple and popular circuit [3]-[8]. However, by its principle, RCD snubber dissipates all of the energy absorbed by the snubber capacitor. As a result, the power loss of RCD snubber is rather significant and, hence, this snubber cannot meet high efficiency requirements of modern power supplies. In quest of improving the efficiency a considerable effort is dedicated to developing simple yet effective

snubber topologies. A variety of “lossless” snubbers were reported in literature, which can limit the peak stress and rate of rise of voltage across the switching device [9]-[16] as well as recycle the absorbed energy.

The non-dissipative LC snubber, shown in Fig. 1 (b), can recycle the captured energy as well as provide favorable turn off conditions for the main switch [17]-[19]. The non-dissipative LC snubber can appreciably improve the efficiency, however, as compared to RCD snubber, requires an additional inductor that increases the component count and cost.

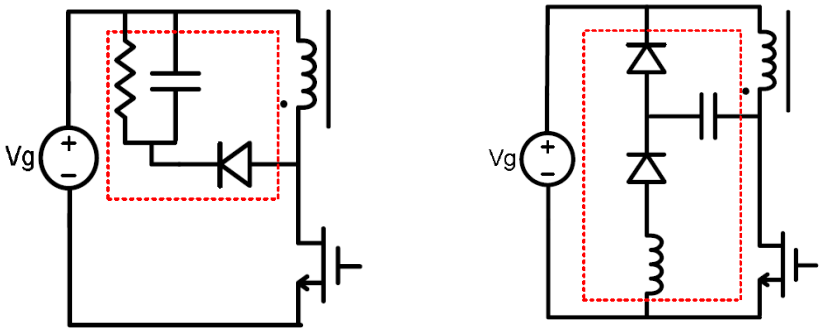

Fig. 1. (a) Dissipative RCD snubber; (b) non-dissipative LC snubber.

Continuous research on soft switching techniques in University of California, Irvine, resulted in several novel snubber topologies [20]-[27]. The recently introduced energy regenerative snubber [24], shown in Fig. 2, can recover the energy captured by the snubber capacitor to the dc bus and, thus, help improve converter’s efficiency. In addition to the advantage of energy recycling, the snubber has lower component count as it does not need a discrete inductor. Instead, the energy regenerative snubber employs transformer’s auxiliary winding and beneficially exploits the transformer’s leakage inductance as a part of the snubber circuit. Hence, both the magnetic core and the associated pcb footprint area can be spared.

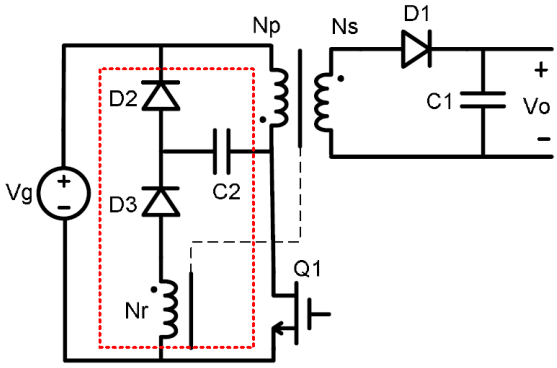

Fig. 2. Topology of the Flyback converter with energy regenerative snubber.

In this paper, the energy regenerative snubber [26] is reviewed and analyzed applying the state plane approach. State plane method is a graphical technique where the state variables are sketched in a two dimensional diagram. This approach has the advantage of visualizing the state trajectory, providing more insight into the ongoing processes. Viewing the circuit behavior in the state-plane is helpful in deriving exact solution. The presented analysis of the energy regenerating snubber by state-plane approach were aimed to provide an accurate and straight forward engineering design procedure that is easy to apply in practice. In addition, to evaluate the performance of the energy regenerative snubber a prototype off-line flyback converter was designed, built and tested. The prototype was fitted with different snubbers and its efficiency performance measured in each case. In comparison with its counterparts, the energy regenerative snubber was found to be more efficient yielding 8% improvement in average over RCD snubber and 2% improvement over non-dispative LC snubber.

The paper is organized as follows: section II of the paper presents a qualitative description and equivalent circuits of operational states of the flyback converter with energy regenerating snuber, section III introduces the adopted notation and normalization and some other basic formula that is later used in quantitative state plane analysis presented in section VI. Design considerations are given in section V. Experimental results are reported in section VI followed by conclusions section. Design example is included in the appendix.

II. Topology, Basic Assumptions and Operation Principles of the Energy Regenerative Snubber

Flyback converter with energy regenerative snubber is shown in Fig. 2. The energy regenerative snubber is comprised of the tertiary transformer winding N_r, snubber diodes D_2, D_3, and the snubber capacitor C_2. The transformer turns ratio is designated as

$$n_s = \frac{N_s}{N_p} \qquad (1a)$$

$$n_r = \frac{N_r}{N_p} \qquad (1b)$$

Where, N_p and N_s are the number of turns of the primary and of the secondary windings respectively.

The basic assumptions in this study are that the circuit is comprised of ideal elements. That is, ideal semiconductor switches are assumed, with negligible voltage drop, delays, and capacitances. Also, the output voltage ripple is considered negligible so that the output filter capacitor, C_1, can be represented by an equivalent dc voltage source. It is also assumed that the

dominant parameters of the step down transformer are the magnetizing inductance, L_m, and the primary winding leakage inductance, L_{lk}, whereas the secondary and tertiary leakage inductances can be neglected. The magnetizing inductance of the transformer, L_m, is considered large, however, current ripple of the magnetizing inductor will be taken into consideration.

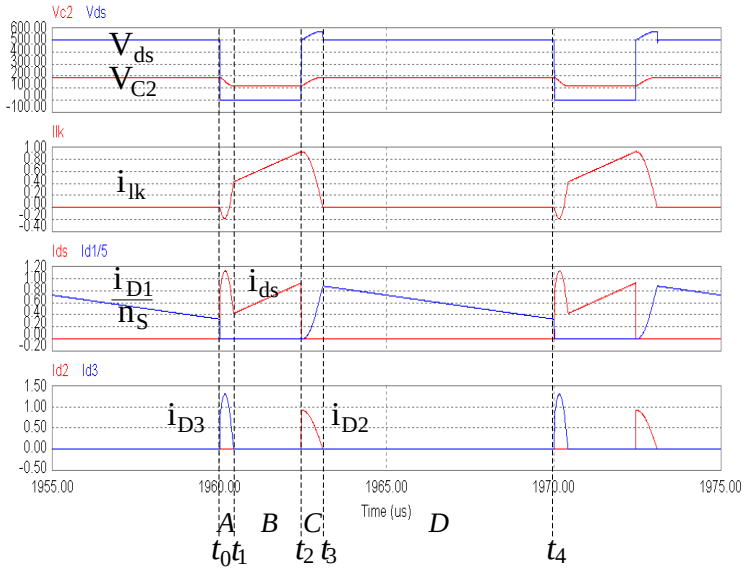

Fig. 3. Simulated waveforms of the flyback converter with energy regenerative snubber in the preferred mode of operation.

Simulated waveforms of the flyback converter with energy regenerative snubber operating in its preferred mode of operation are shown in Fig. 3. Four topological states can be identified within one switching cycle. These topological states arise as a result of conduction modes of the semiconductor devices, which are summarized in Table I.

Table I. Summary of the conduction modes.

	t_0-t_1	t_1-t_2	t_2-t_3	t_3-t_4
Q_1	on	on	off	off
D_1	off	off	on	on
D_2	off	off	on	off
D_3	on	off	off	off

State A - Regenerating, t_0-t_1. This state commences as the switch, Q_1, is turned on by controller command. The sub-topology of this state is shown in Fig. 4 (a) and its equivalent circuit, referred to the N_r winding, is shown in Fig. 4 (b). Here, the dc voltage, V_g, is applied on transformer primary, across L_m and L_{lk}. In addition, the snubber diode, D_3, conducts and C_2

discharges through Q_1 and reset winding N_r. Since the duration of the regenerating state is much shorter than the switching period, the variations in magnetizing current during this state can be neglected. Hence, the magnetizing current in Fig. 4 (b) is represented by a constant current source I_{min}/n_r. This state terminates as D_3 ceases conducting at the instant the capacitor current drops to zero, i_{C2} =0, and the snubber capacitor voltage, V_{C2}, falls to its minimum value, V_{min}.

State B- Charging, t_1-t_2. This state commences as D_3 ceases conducting. The sub-topology of this state is shown in Fig. 4 (c) and its equivalent circuit, referred to the N_p winding, is shown in Fig. 4 (d). Here, the magnetizing and leakage inductances, L_m and L_{lk}, are linearly charged by the dc source, V_g, whereas, the snubber circuit remains idle with the snubber capacitor voltage, V_{C2}, at constant value, V_{min}. This state terminates when the switch, Q_1, is turned off by the controller, at which instant the magnetizing inductance current raises to its maximum value of I_{max}.

State C- Snubbing, t_2-t_3. This state commences as Q_1 is turned off, subject to the condition $V_{min} \geq V_o/n_s$, which is assumed to be fulfilled in a properly designed snubber. The sub-topology of this state is shown in Fig. 4 (e) and its equivalent circuit, referred to the N_p winding, is shown in Fig. 4 (f). Here, the snubber diode, D_2, conducts and the energy stored in the leakage inductance, L_{lk}, is discharged and captured by the snubber capacitor, C_2, which also limits the peak voltage across the switch. The output rectifier, D_1, conducts the reflected to secondary current difference $i_{D1} = i'_{Lm} - i'_{L_{lk}}$, which flows into the output filter capacitance, C_1. Snubbing state terminates as the current through the leakage inductor falls to zero, at which instant the snubber capacitor voltage, V_{C2}, raises to its maximum value of V_{max} and output rectifier current raises to the full magnitude of the referred to the secondary magnetizing current $i_{D1} = i'_{Lm}$.

State D- Discharging, t3-t4. This state commences as the leakage inductor current ceases. The sub-topology of this state is shown in Fig. 4 (g) and its equivalent circuit, referred to the N_p winding, is shown in Fig. 4 (h). Here, the magnetizing inductance, L_m, linearly discharges into the output capacitance C_1 via transformer secondary, whereas, the snubber circuit remains idle preserving the snubber capacitor voltage, V_{C2}, at constant value, V_{max}. Discharging state is terminated at the instant the controller issues the next turn-on command to the switch, at which instant the magnetizing inductance current falls to its minimum value of I_{min}.

In the converter's steady state the whole processes of four intervals repeats in each cycle.

Note, that a state, where only D_2 is on, can exist in between State-B and State-C. The "only D_2 on" state steers the energy into the snubber capacitor, C_2, instead it being transferred to the output circuit and, therefore, is undesirable. This state can be avoided by a proper choice of the snubber capacitor, C_2, which voltage, V_{c2}, is made higher than the reflected output voltage so

that both D_1 and D_2 can turn on at the same time. Simulated waveforms in Fig. 3 show this preferred mode of operation where, both diode D_1 and D_2 conduct in State C, immediately after State B.

In practice, charging of the switch capacitance introduces an additional state. However, here, the analysis is performed under the simplifying assumption of an ideal switch, with negligible switch capacitance, hence, such state will not be considered. This assumption is justified by experimental results which show that the duration and effect of this additional interval are indeed negligible.

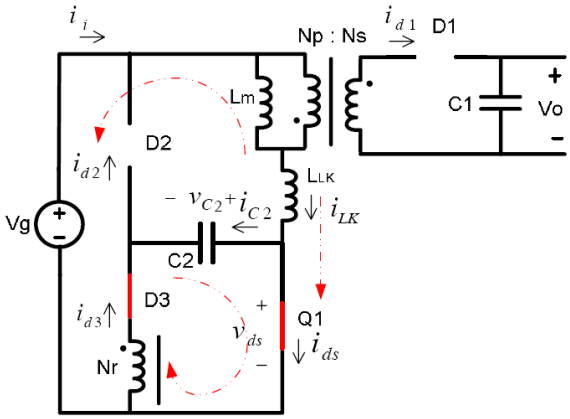

(a)

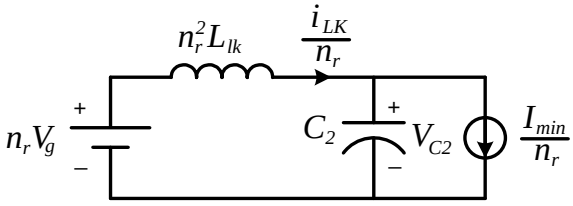

(b)

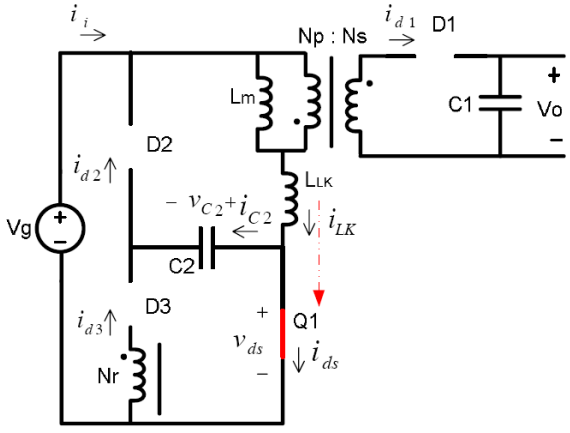

(c)

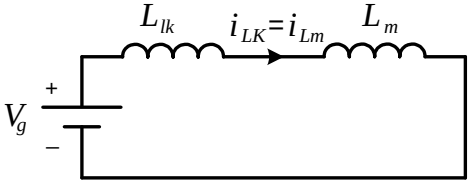

(d)

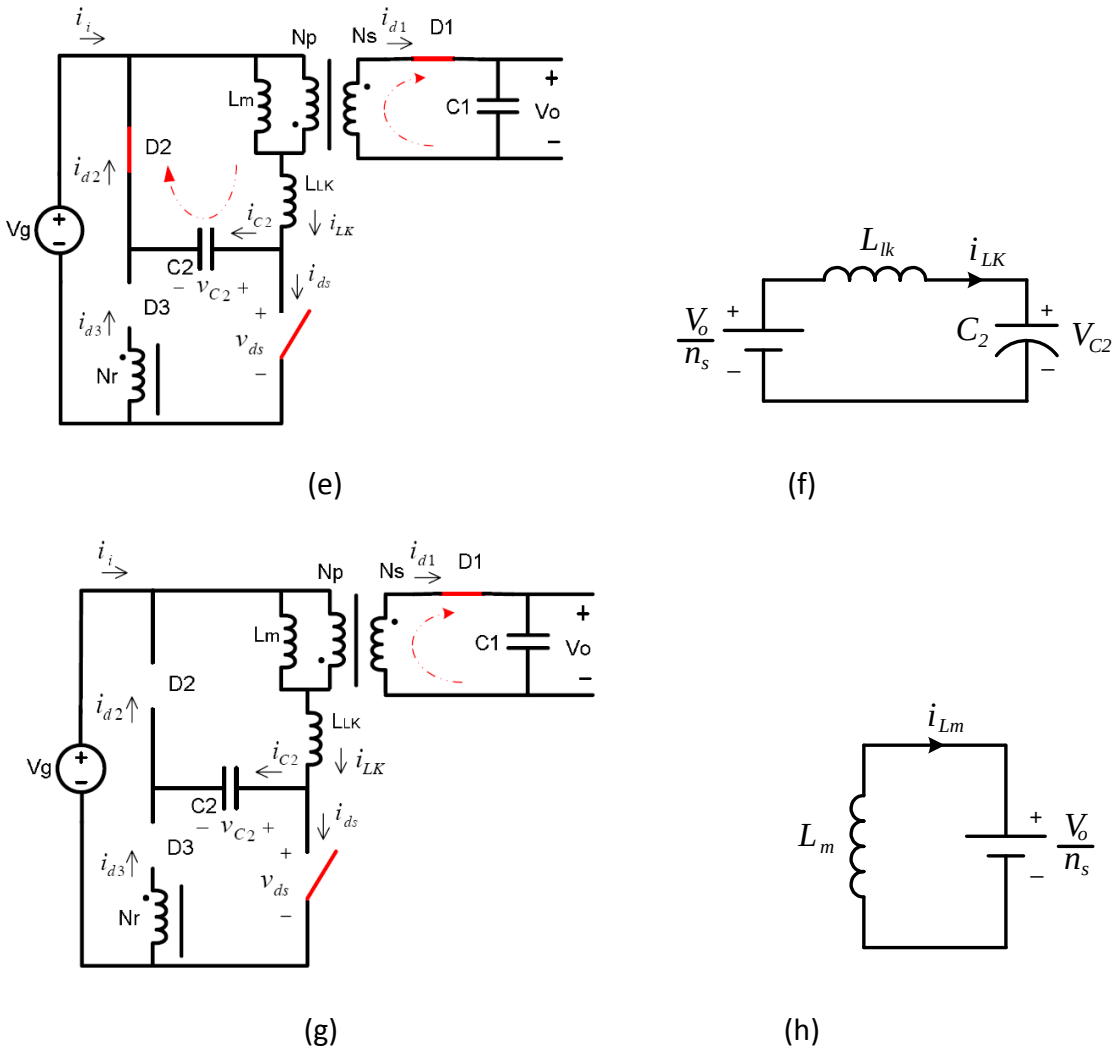

Fig. 4. Topological states of the flyback converter with energy regenerative snubber and their equivalent circuits: (a) Regenerating state; (b) Charging state; (c) Snubbing state; (d) Discharging state.

III. Notation, Normalization and Basics of State Plane Analysis.

This section presents the adopted notation and normalization and reviews basic relationships for later use in quantitative state plane analysis.

Adopting the notation suggested by [28], the complete response of a lossless second order circuit in Fig. 5 (a) can be written in the normalized form as follows:

$$m_C(\theta) = M_T + (m_0 - M_T)\cos\theta + (j_0 - J_T)\sin\theta \qquad (2a)$$

$$j_L(\theta) = J_T + (j_0 - J_T)\cos\theta \ - (m_0 - M_T)\sin\theta \qquad (2b)$$

Here, $\theta = \omega_0 t$ is the angular time and the undamped natural frequency is:

$$\omega_0 = \frac{1}{\sqrt{LC}} \qquad (3)$$

Normalization of voltages in the circuit can be performed with respect to any conveniently chosen base voltage. The most appropriate choice for the base voltage is the input source voltage:

$$V_{base} = V_g \qquad (4)$$

The currents are normalized relatively to a base current, defined as:

$$I_{base} = \frac{V_{base}}{Z_0} = \frac{V_g}{Z_0} \qquad (5)$$

where, the characteristic impedance is:

$$Z_0 = \sqrt{\frac{L}{C}} \qquad (6)$$

Using the notation (3)-(6) above, the normalized capacitor voltage and the normalized inductor current in (2) are defined as:

$$m_C(\theta) = \frac{v_C(\theta)}{V_{base}} = \frac{v_C(\theta)}{V_g} \qquad (7\ a)$$

$$j_L(\theta) = \frac{i_L(\theta)}{I_{base}} = \frac{Z_0 i_L(\theta)}{V_g} \qquad (7\ b)$$

the initial normalized capacitor voltage and the initial normalized inductor current are

$$m_0 = \frac{V_{C0}}{V_{base}} \qquad (8\ a)$$

$$j_0 = \frac{I_{L0}}{I_{base}} \qquad (8\ b)$$

and the normalized voltage and current sources are

$$M_T = \frac{V_T}{V_{base}} \qquad (9\ a)$$

$$J_T = \frac{I_T}{I_{base}} \qquad (9\ b)$$

The normalized solution (2) can be manipulated into a more compact form

$$(m_C(\theta) - M_T)^2 + (j_L(\theta) - J_T)^2 = R^2 \qquad (10)$$

Equation (10) describes a circular arc in the normalized state plane $\left(m_C(\theta), j_L(\theta)\right)$. The solution is centered at point $C = (M_T, J_T)$ and traverses clockwise as shown in Fig. 5 (b). The radii, R, of the arc, which is the amplitude of oscillations in the circuit, depends on the initial conditions and sources value:

$$R^2 = (m_0 - M_T)^2 + (j_0 - J_T)^2 \qquad (11)$$

Time is implicit along this trajectory, however, can be measured by the angle, $\theta = \omega_0 t$, subtended by the arc as shown in Fig. 5 (b).

The usefulness and ease of the state plane technique can be demonstrated by finding the maximum values of the normalized voltage and current. This can be done merely by inspection of Fig. 5 (b):

$$M_{max} = M_T + R \qquad (12\ a)$$

$$J_{max} = J_T + R \qquad (12\ b)$$

Similarly, the minimum normalized voltage and current can be found:

$$M_{min} = M_T - R \qquad (13\ a)$$

$$J_{min} = J_T - R \qquad (13\ b)$$

Simple geometrical considerations also yield the normalized capacitor voltage at zero current crossings of the normalized inductor current as:

$$m_C(j_L = 0) = M_T \pm \sqrt{R^2 - J_T^2} \qquad (14)$$

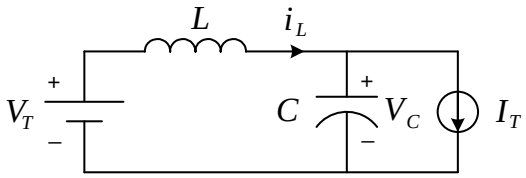

(a)

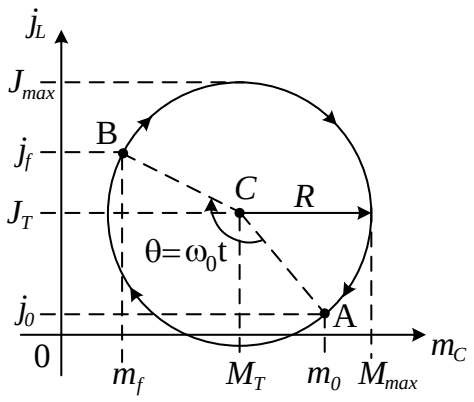

(b)

Fig. 5. (a) A case of a lossless second order system and (b) representation of the circuit response in the normalized state plane.

IV. Analysis of the Regenerative Snubber

This section presents state plane diagram of the snubber and quantitative relationships between the circuit variables. These facilitate derivation of snubber's voltage and current stresses.

The state-plane portrait of the energy regenerating snubber employed by the flyback converter is illustrated in Fig. 6. Here, the horizontal axis represents the normalized snubber capacitor voltage and the vertical axis is the normalized leakage inductance current.

The snubber is activated upon switch transitions, in the regenerating state, see Fig. 4 (a) and (b) and in the snubbing state, Fig. 4 (e) and (f). During these states the snubber equivalent circuit is of a second order and resonates. Thus, according to section III, the state plane trajectory of the snubbing interval can be represented by the arc AB as shown in Fig. 6, whereas, the arc BC represents the regenerating interval.

During the charging interval, see Fig. 4 (d), the snubber capacitor remains idle with constant voltage across it whereas, the leakage inductance current equals the magnetizing inductor current and is linearly rising from its minimum to maximum value. Therefore, the charging interval is represented by the vertical straight line segment CA in Fig. 6.

During the discharging interval both the snubber capacitor and the leakage inductor are idle, with constant voltage, V_{max}, across the snubber capacitor and zero current in the leakage inductance. Hence, throughout the discharging interval the solution rests in point B in Fig. 6.

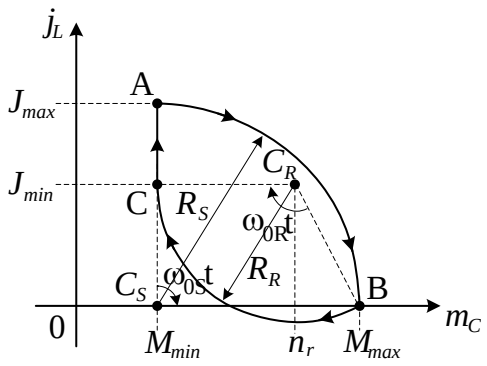

Fig. 6. Normalized state trajectory of the energy regenerative snubber in the preferred mode of operation.

A. Analysis of Snubber Voltage Stress

The presented above state plane diagram is useful in derivation of the snubber voltage stress.

With reference to the generalized circuit in Fig. 5 (a), the normalized sources in the equivalent circuit in Fig. 4 (f), which describes the snubbing interval, assume the values

$$M_T = \frac{V_T}{V_g} = \frac{V_o}{n_s V_g} \qquad (15\ a)$$

$$J_T = \frac{I_T}{V_g/Z_{0S}} = 0 \qquad (15\ b)$$

here, the characteristic impedance is

$$Z_{0S} = \sqrt{\frac{L_{lk}}{C_2}} \qquad (16)$$

The snubbing interval starts at point A with the normalized initial conditions

$$m_0 = M_{min} = \frac{V_{min}}{V_g} \qquad (17\ a)$$

$$j_0 = J_{max} = \frac{I_{max}}{V_g/Z_{0S}} \qquad (17\ b)$$

and terminates at point B, at which instant the final values of the normalized variables equal

$$m_f = M_{max} = \frac{V_{max}}{V_g} \qquad (18\ a)$$

$$j_f = 0 \qquad (18\ b)$$

where, V_g, V_o, V_{max}, V_{min} and I_{max} are as defined in section II above.

Substituting (15) and (17) into (11), the radii of the arc AB in the normalized state plane in Fig. 6 is found as

$$R_S^2 = \left(\frac{V_{min}}{V_g} - \frac{V_o}{n_s V_g}\right)^2 + \left(\frac{Z_{0S} I_{max}}{V_g}\right)^2 \qquad (19)$$

Plugging (18) and (19) into (10) and further manipulating the expression into the ordinary form yields the maximum snubber capacitor voltage

$$V_{max} = \frac{V_o}{n_s} + \sqrt{\left(V_{min} - \frac{V_o}{n_s}\right)^2 + (Z_{0S} I_{max})^2} \qquad (20)$$

Note that during conduction of D_2, see Fig. 4 (e), the voltage of the snubber capacitor (20) adds to the source voltage so that the resulting peak stress across the switch is given by

$$V_{DSpk} = V_g + V_{max} \qquad (21)$$

By inspection of Fig. 6 the duration of the snubbing state is a quarter of a cycle of the resonant ω_{0s} frequency:

$$t_{sn} = \frac{\pi}{2\omega_{0s}} = \frac{\pi}{2}\sqrt{L_{lk} C_2} \qquad (22)$$

With reference to the generalized circuit in Fig. 5 (a), the normalized sources in Fig. 4 (b), which describes the regeneration interval, assume the values

$$M_T = \frac{V_T}{V_g} = \frac{n_r V_g}{V_g} = n_r \qquad (23\ a)$$

$$J_T = \frac{I_T}{V_g / Z_{0R}} = \frac{I_{min}/n_r}{V_g / Z_{0R}} = \frac{Z_{0S} I_{min}}{V_g} \qquad (23\ b)$$

Here, I_{min}/n_r is the minimum value of the magnetizing current at switch turn on instant referred to N_r winding. Also note that here the characteristic impedance is defined as

$$Z_{0R} = \sqrt{\frac{n_r^2 L_{lk}}{C_2}} = n_r Z_{0S} \qquad (24)$$

here, (16) was used.

The regenerating interval starts at point B in Fig 6 with the normalized initial conditions

$$m_0 = M_{max} = \frac{V_{max}}{V_g} \qquad (25\ a)$$

$$j_0 = 0 \qquad (25\ b)$$

and terminates at point C in Fig. 6, at which instant the final values of the normalized variables equal

$$m_f = M_{min} = \frac{V_{min}}{V_g} \qquad (26\ a)$$

$$j_f = \frac{I_{min}/n_r}{V_g/Z_{0R}} = \frac{Z_{0S}I_{min}}{V_g} \qquad (26\ b)$$

Fortunately, the expressions of the normalized currents (15 b), (17 b), (23 b), and (26 b) have the same normalizing coefficients in both snubbing and regenerating states. For this reason both AB and BC arcs appear as circular segments in the state plane in Fig 6. Substitution of (23) and (25) into (11), gives the radii of the arc BC in the normalized state plane

$$R_R^2 = \left(\frac{V_{max}}{V_g} - n_r\right)^2 + \left(\frac{Z_{0S}I_{min}}{V_g}\right)^2 \qquad (27)$$

Plugging (26) and (27) into (10) and further manipulation yields the expression of the minimum snubber capacitor voltage

$$V_{min} = n_r V_g - \sqrt{\left(V_{max} - n_r V_g\right)^2 + (Z_{0S}I_{min})^2} \qquad (28)$$

By inspection of Fig. 6 the duration of the regenerating state is less than half the resonant cycle of ω_{0R} frequency

$$t_{rg} \leq \frac{\pi}{\omega_{0R}} = \pi n_r \sqrt{L_{lk}C_2} \qquad (29)$$

This completes the derivation of two key parameters of the snubber V_{max}, (20) and V_{min} (28).

B. Analysis of Snubber Current Stress

Regeneration of the captured energy back to the dc source manifests itself by the negative current of the leakage inductor, see Fig. 3. The negative peak of the leakage current during the regenerating state is the lowest point on the arc BC in Fig. 6 and can be found substituting (23 b) and (27) into (13 b), and then transforming the normalized expression into the ordinary form

$$I_{lk\_min} = \frac{V_g}{Z_{0s}}(J_T - R_R) = I_{min} - \sqrt{\left(\frac{V_{max} - n_r V_g}{Z_{os}}\right)^2 + I_{min}^2} \qquad (30)$$

Inspecting Fig. 4 (b) and using (30) the peak snubber capacitor current during the regenerating state can be found

$$I_{C2\_pkR} = \frac{1}{n_r}\left(I_{lk\_min} - I_{min}\right) \quad (31)$$

Further inspection of Fig. 4 (a) leads to the derivation of the peak switch current during regenerating state as

$$I_{ds\_pk} = I_{lk\_min} - I_{C2\_pkR} = \left(1 - \frac{1}{n_r}\right) I_{lk\_min} + \frac{I_{min}}{n_r} \quad (32)$$

Note that in the regenerating state both (30) and (31) are of negative polarity, however, since $n_r < 1$ the switch current (32) is positive.

During the snubbing state the peak snubber capacitor current, see Fig.3, is simply

$$I_{C2\_pkS} = I_{max} \quad (33)$$

V. Design Considerations

In this section several practical constrains are suggested that lead to formulation of snubber design rules. Snubber design is the last step in power stage design and is attempted after the values of other circuit parameters, such as n_s, L_m, L_{lk}, and full power I_{min}, and I_{max} were obtained. One possible design approach is as follows. As a first pass design, choose a switch with a reasonable V_{DSmax} for given application. Allowing 20% margin for transient condition the desired maximum snubber voltage can be estimated rearranging (21) as

$$V_{max} \cong 0.8V_{DSmax} - V_g \quad (34)$$

Inspection of (20) suggests that designing the snubber under the condition

$$V_{min} = \frac{V_o}{n_s} \quad (35)$$

results in lowest maximum snubber capacitor voltage

$$V_{\max} = \frac{V_o}{n_s} + Z_{0S} I_{max} \quad (36)$$

Combining (16) and (36) yields the corresponding snubber capacitance as:

$$C_2 = \frac{L_{lk} I_{max}^2}{\left(V_{\max} - \frac{V_o}{n_s}\right)^2} \quad (37)$$

Further inspection of (30) and (32) suggests that designing the snubber under the condition

$$n_r = \frac{V_{max}}{V_g} \quad (38)$$

results in zero minimum leakage current I_{lk_min} (30) and, consequently, lowest peak switch current I_{ds_pk} (32) and lower associated switching losses. This also means that lesser amount of energy is circulating in the circuit which, therefore, can operate with higher efficiency.

For proper circuit operation duty cycle limitation should be respected. Therefore, it is recommended that (22) and (29) should be checked to verify that duration of snubber active states is suficiently shorter than minimum expected controller on and off times T_{ONmin}, T_{OFFmin}:

$$t_{rg} \leq 0.25T_{ONmin} \qquad (39)$$

$$t_{sn} \leq 0.25T_{OFFmin} \qquad (40)$$

Next, rms current rating of snubber components is considered.

Since D_2 conducts the snubber capacitor current in the snubbing state, (22) and (33) can be used to derive the rms current rating of D_2

$$I_{D2rms} = \frac{1}{\sqrt{2}} I_{max} \sqrt{\frac{t_{sn}}{T_s}} \qquad (41)$$

During the regenerating state the snubber capacitor current is carried by D_3. Here, the current appears as a sinusoidal segment, see Fig. 3, for which the peak value is given by (31). Using the upper bound of (29) allows approximating the D_3 rms current as

$$I_{D3rms} = \frac{1}{\sqrt{2}} I_{C2\_pkR} \sqrt{\frac{t_{rg}}{T_s}} \qquad (42)$$

The rms current rating of the N_r winding is the same as (42).

Combining (41) and (42) yields the snubber capacitor rms current

$$I_{C2\_rms} = \sqrt{I_{D2rms}^2 + I_{D3rms}^2} \qquad (43)$$

Assuming that $t_{rg} < T_{on}$, the switch rms current can be approximated by

$$I_{ds_{rms}} \approx \sqrt{\frac{1}{2} I_{ds\_pk}^2 \frac{t_{rg}}{T_{on}} + \frac{D}{3}(I_{max}^2 + I_{max} I_{min} + I_{min}^2)} \qquad (44)$$

The suggested procedure provides a good starting point for first pass design, which can be fine tuned through simulation and prototyping. Design example is given in the appendix.

VI. Experimental Results and Performance Evaluation

The experimental part of this study was dedicated to evaluate the efficiency and compare the performance of the energy regenerating snubber to that of the traditional RCD and the LC non-dissipative snubbers. To attain the experimental results a prototype flyback converter was built and tested. The circuit was designed with the following specifications: Input voltage range- 300V ~ 400V; output voltage- 24V; maximum output power- 50W; switching frequency- 100kHz.

Experimental results were compared to the PSIM simulation program plots used to study the performance of the circuit. Inspection of Fig. 7 - Fig. 10, reveals that the practical circuit behavior closely replicates the predicted. This helps identify in practice the above mentioned topological states and verify the validity of theoretical analysis. Simulation and experimental waveforms shown below are given in the same scale. Clearly seen in Fig. 8 is the t_0-t_1 interval which is the period when clamp capacitor C_2 discharges through Q_1, N_r and D_3, while C_2 and L_{lk} resonate. The current of C_2 resembles a half sine wave and the voltage of C_2 resembles a half cosine wave. Within t_2 -t_3 interval the snubber is in snubbing state, see Fig. 7. During this time, the energy stored in leakage inductance is absorbed by C_2, Consequently Vc2 voltage rises and while the leakage current falls. This is manifested by a gradual drain-to source voltage-rise, visible in Fig. 7, after the MOSFET turn-off. The ringing in the switch voltage and current waveforms seen in Figs. 7 and 8 is due to the switch capacitance and secondary leakage inductance, which were neglected in course of analysis. Comparison of snubber capacitor voltage and current is shown in Fig. 9. Here one can clearly see both the snubber charging the t_2-t_3 interval (absorbing the leakage energy) and discharging, the t_0-t_1 interval, (recycling energy) states. Experimental waveforms are in accordance with the theoretical expectations and simulation.

Performance of the energy regenerative snubber was evaluated experimentally in comparison with other snubbers. The design parameters of RCD, non-dissipative LC and energy regenerative snubbers used in the experiments are summarized in Table II, Table III and Table IV respectively. These snubbers were fitted on the same flyback converter prototype. The efficiency of the prototype with different snuber circuits was measured under the same operating conditions. The resulting efficiency plots are shown in Fig. 10. The overall efficiency of energy regenerative snubber was found to be about 8% higher than that of RCD and about 2 % higher than that of the non-dissipative LC snubber. Apparently, with the non-dissipative snubber the captured energy can only be recycled back to the source, whereas with the energy regenerative snubber some of the energy is fed forward to the output. Thus, energy regenerative snubber has a reduced energy circulation, which results in higher efficiency.

Table II. The parameters of experimental flyback with RCD snubber.

N_p	N_s	L_m	L_{lk}	R_{snb}	C_{snb}
74	11	2.33mH	36.3uH	20kΩ	100nF

Table III. The parameters of experimental flyback with Non-dissipative LC snubber.

N_p	N_s	L_m	L_{lk}	L_{snb}	C_{snb}
74	11	2.33mH	36.3uH	4.5uΩ	1nF

Table IV. The parameters of experimental flyback with energy regenerative snubber.

N_p	N_s	N_r	L_m	L_{lk}	C_{snb}
74	11	48	2.33mH	36.3uH	10nF

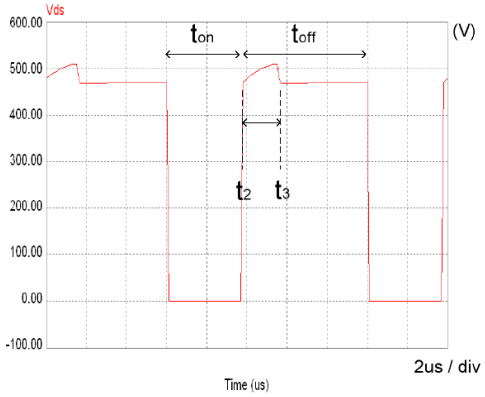

(a)

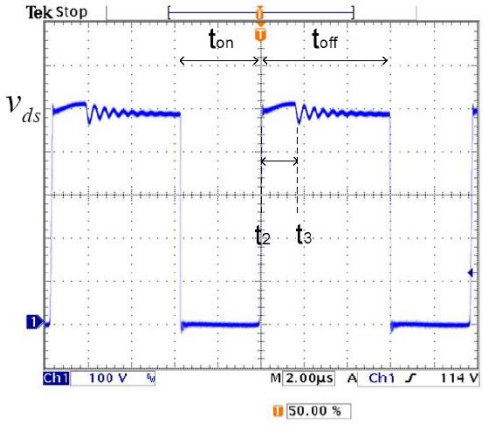

(b)

Fig. 7. Switch voltage, Vds, waveforms: (a) simulated; (b) experimentally measured. Vertical scale: 100 [V/div]; horizontal scale: 2[uSec/div].

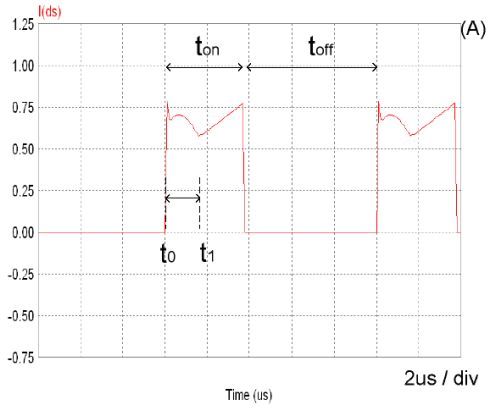

(a)

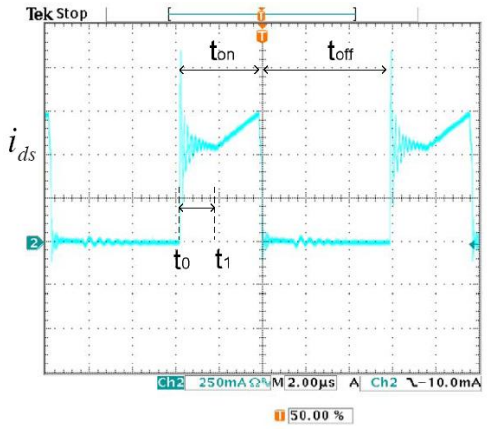

(b)

Fig. 8. Switch current, i_{ds}, waveforms: (a) simulated; (b) experimentally measured. Vertical scale: 250 [mA/div]; horizontal scale: 2[uSec/div].

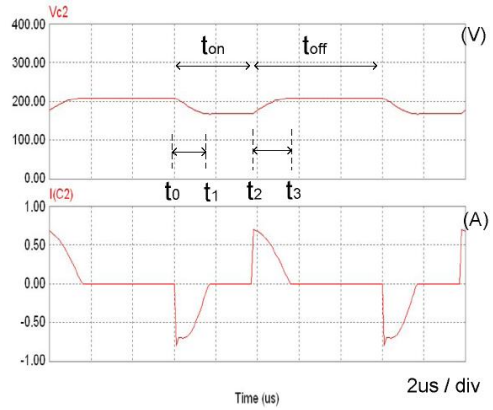

(a)

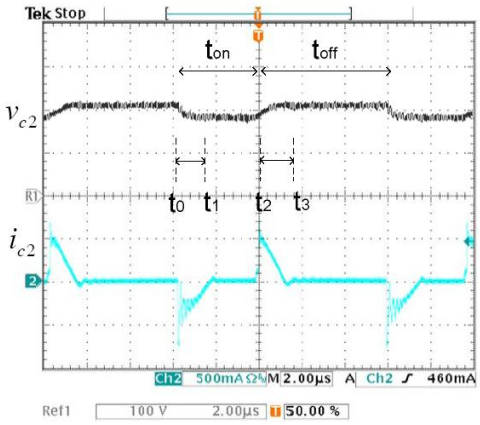

(b)

Fig. 9. Snubber capacitor voltage, V_{C2}, (top trace) and current i_{C2} (bottom trace): (a) simulated; (b) experimentally measured. Vertical scale: top trace 100 [V/div]; bottom trace 500 [mA/div]; horizontal scale: 2[uSec/div].

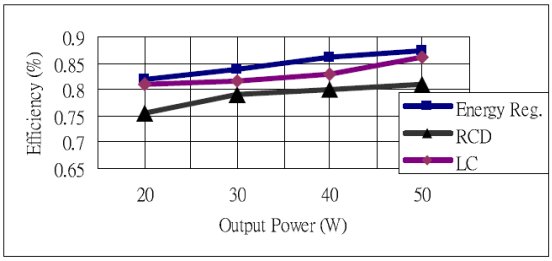

Fig. 10. Efficiency comparison of flyback converter with RCD, non-dissipative,

and energy regenerative snubbers.

CONCLUSION

This paper examined the energy regenerating snubber suited for the flyback converter. Off-line flyback is one of the more popular and wide used topologies and is a good application example for the snubber since the transformer primary leakage is substantial and can be beneficially exploited as a part of the snubber circuit.

Preliminary snubber analysis and design procedure were suggested earlier by [26]. The preliminary analysis relied on simplified assumptions and provided a set of inequalities as

guidance for choosing the snubber parameters. This necessitated a trial and error approach to fine tune the design. This weakness motivated the present study of the snubber using a different analytical method to revise the theory and the design procedure. The presented analysis of the energy regenerative snubber by the state plane approach yielded an accurate and straight forward engineering design procedure that is easy to apply in practice. Although a single output converter was examined here, the snubber operation principles and design rulles are applicable to multi-winding case as well.

Snubber design is a multi-objective optimization procedure that aims to minimize switch voltage and current stresses, under given input voltage and load current range, provide a zero-voltage switching in a wide range, and maximize the efficiency. Same snubber circuit applied to other topologies may have different operating modes and, consequently, different performance. Therefore, a snubber can be fairly assessed and compared in a specific application. Comparative experimental performance evaluation of the energy regenerative snubber was performed on a prototype off-line flyback converter. The prototype was fitted also with RCD and non-dissipative LC snubbers and its efficiency performance measured in each case. With an RCD snubber, the voltage stress of the switch and the power dissipation of the snubber are a trade-off. Both are determined by the value of snubber resistor. The high power dissipation has long been its drawback. The non-dissipative LC snubber can significantly reduce the loss of snubber circuit; however, an extra inductor for the snubber increases the cost and makes design more complicated. In comparison, the voltage stress of the energy regenerative snubber is set by the turns of reset winding N_r without sacrificing efficiency. The hidden feature of this energy regenerative snubber is the beneficial use it makes of the transformer leakage inductance. Moreover, the tertiary winding shares the same core with the transformer, which is cost effective as neither dedicated core nor pcb footprint area are required for a discrete inductor. Inspection of the experimental efficiency plot, shown in Fig. 10, reveals that under the same voltage stress the efficiency of energy regenerative snubber has 8% improvement in average over RCD snubber and 2% improvement over non-dissipative LC snubber.

The reported snubber was patented and successfully commercialized. The improved designing procedure suggested here can help designers to incorporate the regenerative snubber topology in their new products with the potential benefit of increased and wider use of energy efficient and eco-friendly power converters in industry.

Last but not least, as far as engineering education is concerned, the relative simplicity of the regenerative snubber circuit makes it a suitable study-case for teaching the subject of soft-switched power converters and advanced analytical techniques in graduate level courses. In fact, this circuit was included in the curricula of EECS267B “Industrial and Power Electronics” course offered to graduate students in University of Caifornia, Irvine.

APPENDIX: Design example

This step by step design example demonstrates the application of the regenerative snubber design procedure derived earlier in the paper.

Objective: design a regenerating snubber for a given isolated flyback converter. Operating conditions are: input voltage is V_g=380Vdc, output voltage is V_o=24Vdc, output power is Po =150W. Transformer secondary turns ratio is n_s=10/50=0.2; magnetizing inductance is L_m=1.5mH; and the primary leakage inductance is L_{lk}=30uH. The switching frequency is f_s=100kHz. Deliverables: determine the snubber capacitor C_2 and the tertiary turns ratio n_r.

As a first step the basic operation conditions are calculated: the required duty cycle ratio is $D = V_o/(V_o + n_s V_g) = 0.24$. The average output current is: $I_o = P_o/V_o = 6.25A$; average magnetizing inductor current is: $I_{Lm} = n_s I_o/(1-D)$ =1.65A; and the magnetizing current ripple is $\Delta I = DV_g/L_m f_s = 0.6A$. So that the maximum value of the magnetizing current is I_{max} =1.95A; and the minimum value of magnetizing current is I_{min} =1.35A.

Second step: snubber operating conditions and parameters are calculated following the proposed above design procedure. Assuming that the switch is rated V_{DSmax}=800V the maximum snubber capacitor voltage is found from (34) as V_{max}=260V and the minimum snubber capacitor voltage from (35) as V_{min}=120V. Using the given above data for L_{lk}, I_{max}, V_{max}, V_o, and n_s, the snubber capacitance is calculated using (37) as C_2=5.813nF. The transformer tertiary turns ratio is calculated from (38) as n_r=0.684. Current rating of the devices can be then found using (39)-(44).

This design example was simulated in PSIM software. Table V presents the comparison of calculated and simulated results. Excellent agreement is found. The drop in the output voltage is due to the leakage inductance impeding the output rectifier current.

Table V. Design example: comparison of calculated and simulated results.

Parameter	Calculated	Simulated
V_o [V]	24	23.14
V_{DSpk} [V]	640	637.8
V_{max} [V]	260	258.2
V_{min} [V]	120	156.6
I_{max} [A]	1.95	1.92
I_{min} [A]	1.35	1.36
I_{lk_min} [A]	0	0.018
I_{C2pkR} [A]	-1.96	-1.99

I_{DSpk} [A]	1.96	2.00

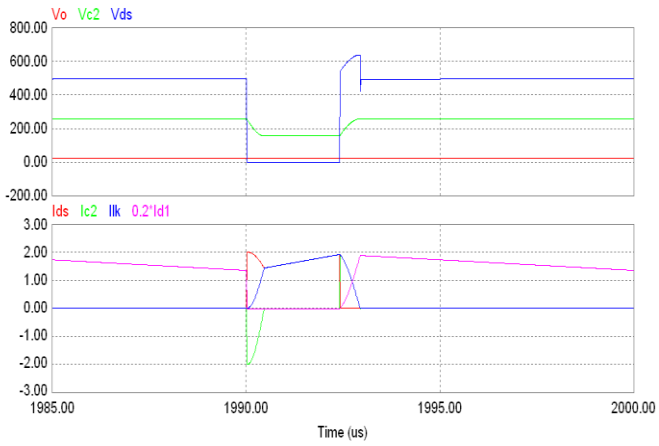

Fig. 11. Design example: simulated waveforms.

REFERENCES

[1] R. W. Ericson and D. Maksimovic, *Fundamentals of Power Electronics*, 2nd ed. Norwell, MA: Kluwer, 2000.

[2] N. Mohan, T. M. Undeland, and W. P. Robbins, *Power Electronics; Converter, Applications and Design*, 3rd ed. New York: Wiley, 1989.

[3] K. Harada, T. Ninomiya, and M. Kohno, "Optimum design of *RC* snubbers for switching regulators," *IEEE Trans. Aerosp. Electron. Syst.*, vol. AES-15, pp. 209-218, Mar. 1979.

[4] S. J. Fenney, B. W.Williams and T. C. Green "RCD Snubber Revisited," *IEEE Trans. Ind. Appl.*, vol. 32 no. 1, pp.155-160, Jan/Feb 1996.

[5] A. Hren, J. Korelic, andM.Milanovic, "RC-RCD clamp circuit for ringing losses reduction in a flyback converter," *IEEE Trans. Circuits Syst. II, Exp. Briefs*, vol. 53, no. 5, pp. 369–373, May 2006.

[6] R. Severns, "Design of Snubbers for Power Circuits," available on line http://www.cde.com/tech/design.pdf.

[7] G-B Koo, "Design Guidelines for RCD Snubber of Flyback Converters," Fairchild Semiconductor Application Note AN-4147, available on line http://www.fairchildsemi.com/an/AN/AN-4147.pdf

[8] --- ---, "Snubber Circuits Suppress Voltage Transient Spikes in Multiple Output DC-DC Flyback Converter Power Supplies", Maxim Tutorial 848, Nov. 12, 2001, available on line http://www.maxim-ic.com/appnotes.cfm/appnote_number/848.

[9] Fan, S.-Y. Tseng, S.-Y. Chang, G.-K. "Multi-output auxiliary power supply with lossless snubber" IEEE Conference on Industrial Electronics and Applications (ICIEA), 2011, 21-23 June 2011, pp. 2172 – 2178.

[10] N. Rouger, J. C. Crebier, and S. Catellani, "High-efficiency and fully integrated self-powering technique for intelligent switch-based flyback converters," *IEEE Trans. Ind. Appl.*, vol. 44, no. 3, pp. 826–835, May/Jun 2008.

[11] Y. B. Weng and Y. Xing, "A dual-transformer flyback converter in critical conduction mode," in *Proc. IEEE IPEMC*, 2004, vol. 3, pp. 1074–1079.

[12] C. Y. Inaba, Y. Konishi, H. Tanimatsu, K. Hirachi, and M. Nakaoka, "Soft switching PWM DC–DC flyback converter with transformer-assisted pulse current regenerative passive resonant snubbers," in *Proc. IEEE PEDS*, 2003, vol. 2, pp. 882–887.

[13] M. Jinno, P.-Y. Chen, and K.-C. Lin, "An efficient active LC snubber for multi-output converters with flyback synchronous rectifier," in *Proc. IEEE PESC*, 2003, vol. 2, pp. 622–627.

[14] K.-B. Park, C.-E. Kim, G.-W. Moon, and M.-J. Youn, "New cost-effective PWM single-switch isolated converter," in *Proc. IEEE PESC*, 2007, pp. 1715–1720.

[15] A. Bakkali, P. Alou, J. A. Oliver, and J. A. Cobos, "Average modeling and analysis of a flyback with active clamp topology based on a very simple transformer," in *Proc. IEEE APEC*, 2007, pp. 500–506.

[16] C. Munoz, "Study of a new passive lossless turn-off snubber," in Proceedings of the CIEP Conference, 1998, pp.147-152.

[17] M. Domb, R. Redl, N. 0. Sokal, "Nondissipative turn-off snubber alleviates switching power dissipation, 2nd breakdown stress and Vce overshoot: analysis, design procedure and experimental verification," PESC Conf. Proc., 1982, pp. 445-454.

[18] T. Ninomiya, T. Tanaka, K. Harada, "Analysis and Optimization of a Nondissipative LC Tun-Off Snubber," IEEE Trans. on Power Electronics, vol. 3, No. 2, April 1988, pp. 147-156.
[19] T.-H. Ai, “A novel integrated non-dissipative Snubber for flyback converter,” in *Proc. Intern. Conf. Syst. Signals*, 2005, pp. 66–71.
[20] K. M. Smith, Jr. and K. Smedley, “Lossless passive soft switching methods for inverters and amplifiers,” in *IEEE Pesc Conf. Rec.*, 1997, vol. 2, pp. 1431–1439.
[21] K. M. Smith, Jr. and K. M. Smedley, “Properties and synthesis of lossless, passive soft switching converters,” in *1st Int. Congress Israelon Energy, Power & Motion Control Proc.*, May 1997, pp. 112–119.
[22] K. M. Smith and K. Smedley, “Engineering design of lossless, passive soft-switching PWM converters. Part I. With minimum voltage stress circuit cells,” in *IEEE APEC Conf. Rec.*, 1998, vol. 2, pp. 1055–1062.
[23] K. M. Smith, Jr. and K. Smedley, “Engineering design of lossless passive soft switching methods for PWM Converters: Part II,” in *Intelec’98 Conf. Rec.*, Oct. 1998.
[24] K. M. Smith, C. Ji, and K. M. Smedley, “Energy regenerative clamp for flyback Converter”, UCI, invention disclosure, Sept. 1998.
[25] C. Ji, K. M. Smith, Jr., and K. M. Smedley “Cross Regulation in Flyback Converters: Analytic Model and Solution” IEEE Trans. On Power Electronics, Vol. 16, No.2, March 2001.
[26] C.-S. Liao and K. M. Smedley, “Design of high efficiency flyback converter with energy regenerative snubber,” in *Proc. IEEE APEC*, 2008, pp. 796–800.
[27] A. Abramovitz, T. Cheng, and K. Smedley, “Analysis and design of forward converter with energy regenerative snubber,” IEEE Trans. Power Electron., Vol. 25, No. 3, pp. 667-676, Mar. 2010.
[28] R. W. Erickson, “Materials on state plane analysis of resonant converters” available on line “http://ecee.colorado.edu/~ecen5817/notes/stateplane/spa.html.“